RSC Advances

PAPER

View Article Online
View Journal | View Issue

Cite this: *RSC Adv.*, 2025, **15**, 43487

Pyrolysis behaviours and kinetics study of corn ethanol industry co-product towards its bioenergy potential

Gaurav Singh,[a] Ranjeet Kumar Mishra *[b] and Neeraj Kumar*[a]

Distillers Dried Grains with Solubles (DDGS) is a promising bioenergy feedstock owing to its abundant availability and rich organic composition. This study investigates the pyrolysis behaviour of DDGS using thermogravimetric analysis (TGA) at heating rates of 10, 20, and 30 °C min^{-1} to determine its kinetic and thermodynamic parameters. Model-free methods such as Kissinger–Akahira–Sunose (KAS), Flynn–Wall–Ozawa (OFW), Starink (STM), and Vyazovkin (VZM), along with model-fitting approaches such as Coats-Redfern (CR) and Distributed Activation Energy Model (DAEM), were employed to estimate the kinetic parameters. The apparent activation energy (E_a) varied significantly with conversion (α), ranging from 82 to 525 kJ mol^{-1} across different models, confirming the multi-step nature of pyrolysis. Further, CR fitting yielded lower activation energy values of 36.34 and 39.32 kJ mol^{-1} biomass at reaction orders between 1.0 and 2.7. Thermodynamic analysis revealed that enthalpy (ΔH) increased from 84 to 520 kJ mol^{-1} as conversion progressed from 0.1 to 0.8, while Gibbs free energy (ΔG) remained positive (87–233 kJ mol^{-1}), indicating a non-spontaneous process requiring external energy. Further, the entropy (ΔS) shifted from negative values at low conversions (−111 J mol^{-1} K^{-1}) to highly positive values at higher conversions (up to 573 J mol^{-1} K^{-1}), reflecting increasing molecular disorder. This trend suggests that the later stages of pyrolysis are dominated by lignin degradation and associated structural changes. The obtained results confirm that DDGS pyrolysis follows a complex, multi-step pathway influenced by biochemical composition and inherent minerals. Further, the present study aligns with Sustainable Development Goals (SDGs) 6, 7, 13, 14 and 15.

Received 28th August 2025
Accepted 16th October 2025

DOI: 10.1039/d5ra06424d

rsc.li/rsc-advances

1. Introduction

Distillers' Dried Grains with Solubles (DDGS) is a significant by-product of the liquor, vinegar, and bioethanol industries, produced in substantial quantities. The production of DDGS has surged due to the rapid expansion of the grain-based ethanol industry under the government biofuel blending program. The annual output has increased nearly 13-fold over the past two years, reaching an estimated 5.50 million tons in 2025.[1] The domestic supply of DDGS to the animal feed sector in India was estimated at around 3.20 million metric tons (MMT) in 2024-25 and is projected by the United States Department of Agriculture (USDA) to increase to 4.20 MMT by 2025-26.[2] The exports have also grown significantly, with India shipping approximately 166 070 metric tons in 2023-24, positioning the country as a potential key supplier to markets in the Middle East and Southeast Asia.[1] The increase is supported by the feed industry's preference for DDGS over soybean meal and government policies endorsing multiple grain-based ethanol plants. DDGS is rich in cellulose, hemicellulose, proteins, and amino acids, which serve as key precursors for acidogenesis and methanogenesis, and represent a valuable biomass resource. Despite this, they remain largely underutilised and are often considered waste.[3] Although primarily utilised as animal feed for their rich protein, vitamin, and mineral content, the high moisture and strong acidity of DDGS cause them to spoil quickly under ambient conditions, leading to environmental pollution.[4,5] In the agriculture sector, DDGS are typically dried and composted to underutilise their rich bioactive compounds, leading to resource loss and diminished economic gains for producers. There is growing interest in advanced conversion technologies to transform DDGS into biofuels, biochemicals, and biomaterials owing to their abundance, economic potential, and environmental concerns, thus achieving value addition and efficient resource recovery.[6] Additionally, DDGS is considered carbon neutral, offering notable environmental advantages by lowering the carbon footprint associated with fossil fuel consumption.[7] DDGS possess suitable characteristics to serve as a promising feedstock for pyrolysis. Pyrolysis is a thermal decomposition process carried out under oxygen-deficient

[a]*Department of Applied Sciences, J. B. Institute of Technology, Veer Madho Singh Bhandari Uttarakhand Technical University, Dehradun-248015, India*

[b]*Department of Chemical Engineering, Manipal Institute of Technology, Manipal Academy of Higher Education, Manipal, Karnataka-576104, India. E-mail: ranjeet.mishra@manipal.edu; vatsneeraj78@gmail.com*

conditions at moderate temperatures (400–900 °C) (usually atmospheric pressure).[8] Zhang *et al.* (2018) studied the co-pyrolysis of dried DDGS with waste using a hierarchical ZSM-5/MCM-41 catalyst. They reported that co-pyrolysis produced higher hydrocarbon yields in bio-oil than the pyrolysis of waste plastic or DDGs individually. This enhancement was attributed to the high oxygen content of DDGS, which generates oxygenated compounds in the pyrolytic vapours, promoting chain scission and the breakdown of long-chain organic molecules in waste plastic films.[9] Further, Lv *et al.* (2019) examined the co-gasification of spirit-based distillers' grains (SDGs) with anthracite coal for hydrogen-rich gas production. They reported that adding SDGs increased the hydrogen content of the gas product and the overall gasification reactivity owing to the cracked structure and large surface area of SDGs char formed during thermal decomposition.[5] Therefore, understanding the pyrolysis kinetics of DDGS is essential for elucidating their reaction mechanisms, optimising process parameters, and controlling the design and scale-up of industrial pyrolysis systems.

Thermogravimetric analysis (TGA) has been widely recognised as an effective and efficient tool for elucidating the pyrolysis reaction kinetics of biomass. TGA-based kinetic investigations generally follow two main approaches: isothermal and non-isothermal models.[10] Non-isothermal techniques are generally preferred due to their lower margin of error, as isothermal methods require holding time and heating rates, which can introduce inaccuracies.[11] Non-isothermal analysis also offers concrete advantages, such as reduced experimental time, continuous data acquisition over a broad temperature range, and fewer errors associated with thermo-chemical induction. Non-isothermal techniques are divided into model-fitting and model-free (iso-conversional) approaches. The model-free methods are preferred for their lower error and independence from predefined reaction models.[11] Non-isothermal TGA at lower, dynamic heating rates is especially suitable for predicting pyrolysis kinetics, as higher heating rates may cause turbulence and peak shifts, reducing accuracy.[12] The iso-conversional models determine activation energy (Ea) as a function of heating rate and temperature, often assuming constant Ea and uniform heating throughout the process. They are used to study devolatilization kinetics and assess biomass physicochemical properties.[13] Different kinetic models (two-step, parallel reaction models, three-step multi-pseudo-component models, random nucleation, diffusion, phase-boundary mechanisms and three-step multi-pseudo-component models) have been applied to TGA pyrolysis to understand the kinetic behaviour of biomass.[10]

Thermal analysis often employs iso-conversional techniques to determine the apparent activation energy (E_a) of solid-state reactions without assuming a specific model. The Kissinger–Akahira–Sunose (KAS) and Flynn–Wall–Ozawa (OFW) methods utilise thermogravimetric data obtained at different heating rates through integral approaches. OFW employs Doyle's approximation, while KAS uses a linearization method providing slightly higher accuracy at low conversions. The Distributed Activation Energy Model (DAEM) effectively describes complex materials, such as biomass, by considering multiple concurrent first-order reactions with distributed activation energies.[14] The Starink Method (STM) minimises Doyle's approximation error, enhancing accuracy without adding complexity, while the Vyazovkin Method (VZM) achieves high precision by minimising the temperature–time integral, avoiding linearization. DAEM and VZM are suitable for complex biomass pyrolysis due to their ability to account for variable activation energies, while STM offers a practical balance between simplicity and accuracy. Several studies reported on the kinetic analysis of biomass. Xiao *et al.* (2020) studied the kinetics of rice straw and pine sawdust in a TGA using the Coats-Redfern method, Doyle, and DAEM. They found that the Coats-Redfern method yielded the lowest apparent activation energy, ranging between 30 and 70 kJ mol^{-1}. In contrast, the DAEM and Doyle methods provided comparable values of 67.6, 245.8, and 271.8 kJ mol^{-1} for rice straw, pine sawdust, and Phoenix tree leaves, respectively.[15] Stančin *et al.* (2021) analysed the kinetics of biomass-polyurethane foam mixtures using Friedman, KAS, OFW, and STM. Their findings showed that KAS, OFW, and STM tended to underestimate the activation energy at the initial and final stages, although the values aligned closely within the main conversion range. The highest activation energy values were observed for individual pyrolysis, whereas polyurethane degradation exhibited the lowest.[16] Pal *et al.* (2021) investigated the pyrolysis of *Mangifera indica* L., *Artocarpus heterophyllus* L., and *Syzygium cumini* seeds using TGA at heating rates of 10, 15, 20, 25, and 30 °C min^{-1}. Applying Flynn–Wall–Ozawa, Kissinger–Akahira–Sunose, Vyazovkin, and Vyazovkin AIC methods, they reported apparent activation energies ranging from 179.86 to 226.31 kJ mol^{-1} within 0.1–0.7 fractional conversion range.[17] Kumar *et al.* (2021) carried out a kinetic analysis of peanut shells using a thermogravimetric analyser at heating rates of 10, 15, and 20 °C min^{-1}. They employed Flynn–Ozawa–Wall (OFW), Kissinger–Akahira–Sunose (KAS), Starink, Tang, Vyazovkin, and Vyazovkin AIC methods, and reported activation energy values ranging between 186 and 226.97 kJ mol^{-1}.[18] As per the literature review, it was noticed that previous research has focused largely on lignocellulosic residues such as rice straw, peanut shells, and fruit seeds; however, very limited studies have examined DDGS despite its abundance, high cellulose and protein content, and potential for value-added energy recovery. There is a lack of systematic kinetic and thermodynamic evaluation of DDGS, which hinders optimisation of its conversion pathways and industrial utilisation in bioenergy production. By performing thermogravimetric analysis (TGA) under different heating rates (10–30 °C min) and applying multiple model-free kinetic approaches, this work aims to provide a detailed understanding of apparent activation energy variations, frequency factors, and thermodynamic parameters across conversion ranges. This study lies in exploring the pyrolysis behaviour and kinetic analysis of DDGS using KAS, OFW, DAEM, VZM, and STM.

Therefore, keeping the above-mentioned research gaps, the present work demonstrated the pyrolysis behaviour and kinetic analysis of DDGs using five model-free methods (Kissinger–Akahira–Sunose (KAS), Flynn–Wall–Ozawa (OFW), Distributed

Activation Energy Model (DAEM), Vyazovkin Method (VZM) and String method (STM). The pyrolysis experiment was performed in a thermogravimetric analyser at dynamic heating rates (10, 20 and 30 °C min^{-1}) under an inert atmosphere. Further, the TGA data obtained was fitted into the selected model to estimate the kinetic parameters (apparent activation energy, frequency factor and order of reaction). The physicochemical characterisation of DDGS was performed as per its physical and chemical properties.

2. Materials and methods

2.1. Sample collection and preparations

DDGS were sourced from a local distillery industry near Muzaffarnagar District, Uttar Pradesh, India. The sourced sample was washed with distilled water and sun-dried for 2 days. Further, the sun-dried sample was placed in a hot air oven at 105 °C for 2–3 h for uniform removal of moisture content. The DDGS samples were ground using a multifunction swing pulveriser to obtain particles in the size range of 0.1–0.2 mm. The resulting particles were stored in a desiccator to maintain their integrity prior to physicochemical characterisation and thermogravimetric analysis (TGA).

2.2. Physicochemical characterisation of feedstock

The physicochemical characterisation of the processed DDGS samples was carried out to assess their fundamental properties, including proximate and ultimate analysis, as well as energy content. The proximate analysis was performed in accordance with ASTM standard methods, with the corresponding standards and key apparatus detailed in Table 1. Ultimate analysis was performed using an elemental analyser (PerkinElmer 2400 II, USA) in accordance with ASTM standards E777-87, E778-08, and E775-15 to quantify the carbon (C), hydrogen (H), nitrogen (N), and sulphur (S) contents. The oxygen (O) content was determined by difference, subtracting the combined percentages of carbon, hydrogen, nitrogen, sulphur, and ash from 100 wt%. The detailed analysis of the proximate and elemental composition is reported by Mishra *et al.* (2019).[19] The experiment was repeated three times for better accuracy of the results. Metal analysis of the substrate was performed using Inductively Coupled Plasma-Optical Emission Spectroscopy (ICP-OES) with a PerkinElmer Optima 5300DV instrument, following acid digestion of the samples. The silica content was quantified spectrophotometrically from the ashed samples, following the procedure described by Bridgeman *et al.* (2007).[20] Furthermore, eqn (1)–(4) are used to calculate the base-to-acid ratio, alkali index, iron calcium ratio, and total alkali in the ash content of DDGS. The calorific value (higher heating value, HHV) of DDGS was determined using an Oxygen Bomb Calorimeter (Parr, 6400). The structural components are crucial in pyrolysis kinetic analysis, as each compound decomposes within a specific temperature range. The biochemical composition of the biomass, including hemicellulose, cellulose, and lignin, was analysed using the Van Soest wet chemistry method (Van Soest, 1967).[21] The XRD patterns (crystallinity index) of the biomass samples were recorded using a Rigaku TT Rax diffractometer equipped with a Cu Kα radiation source, operating at 9.0 kW and 250 mA. The scans were performed over a 2θ range of 5–50° at a scanning speed of 0.03 min^{-1} for all biomass samples.

$$\text{Base to acid}\left(\frac{B}{A}\right)\text{ratio} = \frac{\%(Fe_2O_3 + CaO + MgO + K_2O + Na_2O)}{\%(SiO_2 + TiO_2 + Al_2O_3 + P_2O_5)} \quad (1)$$

$$\text{Alkali index(AI)} = \frac{Kg(K_2O + Na_2)}{GJ} \quad (2)$$

$$\text{Iron calcium ratio}\left(\frac{I}{C}\right) = \frac{\%[Fe_2O_3]}{\%[CaO]} \quad (3)$$

$$\text{Total alkalis (TA)} = \%Na_2O + \%K_2O \quad (4)$$

2.3. Thermal decomposition profile analysis

The pyrolysis kinetics of DDGS were studied using a thermogravimetric analyser (TGA, PerkinElmer). High-purity nitrogen was introduced at 20 mL min^{-1} as a protective gas to prevent damage from volatile emissions, while an additional nitrogen flow of 50 mL min^{-1} was used as purge gas to sustain an inert

Table 1 Test standards and main apparatuses for proximate analysis of DDGS

Property (wt%)	Test standard	Apparatus	Procedures
Moisture content	ASTM E1756-08	Rotek hot air oven (250 °C), Mumbai, India	The sample was dried at 105 °C for a minimum duration of 3 h
Volatile matter	ASTM E1755-01	Ants Innovations-2171 Pvt. Ltd, Mumbai, India	The sample was heated to 925 °C and held at that temperature for 7 min
Ash content	ASTM E872-82	Ants Innovations-2171 Pvt. Ltd, Mumbai, India	The sample was heated at 575 °C for a duration of 3 h
Fixed carbon	E870-82		It is calculated by subtracting the combined contents of moisture, ash, and volatile matter from 100 wt%

atmosphere and rapidly remove pyrolysis volatiles. The experiments were carried out with 9 mg of sample at heating rates of 10, 20, and 30 °C min^{-1} within a temperature range of 30–900 °C.

2.4. FTIR analysis

FTIR analysis of the biomass was carried out using an FTS 3500 GX instrument equipped with DRS. The dried sample was mixed with KBr in a 1 : 100 ratio and placed in a sample holder. FTIR spectral scanning was performed with 40 scans per second at a resolution of 4 cm^{-1}, covering the wavenumber range of 400–4000 cm^{-1}.

2.5. Kinetic theory

Isoconversional kinetic methods effectively analyse complex solid-state reactions like biomass pyrolysis by determining activation energy (E_α) without assuming a reaction mechanism. Models such as FWO, KAS, DAEM, STM, and VZM use thermogravimetric data at multiple heating rates to evaluate E_α across conversion levels (α), revealing varying energy barriers during decomposition.[22] Due to the diverse composition of lignocellulosic biomass, pyrolysis involves thousands of simultaneous reactions, making precise mechanism identification challenging, though a general reaction can be represented.

$$\text{Biomass(solid)} \xrightarrow{k(t)} \text{volatile(gases + tar)} + \text{char(solid residue)} \quad (5)$$

It is assumed that the conversion of raw material into product occurs as a single-step process. Accordingly, based on the Arrhenius equation, the reaction rate constant is expressed as

$$k = k_0 e^{-\left(\frac{E}{RT}\right)} \quad (6)$$

where k = reaction rate constant, k_0 = pre-exponential factor, (min^{-1}), E = activation energy, (KJ mol^{-1}), R = gas constant, (8.314 J mol^{-1} K^{-1}), and T = absolute temperature, (K). The rate equation for the conversion of biomass from the solid phase to the volatile phase can be expressed as:

$$\frac{dx}{dt} = k_f(x) \quad (7)$$

where x = rate of conversion within the sample and t = time. The conversion of biomass into fuel is a function of temperature. Thus, the conversion factor is defined as:

$$x = \left(\frac{\alpha_0 - \alpha_t}{\alpha_0 - \alpha_f}\right) \quad (8)$$

where α_0 is the initial weight of biomass, α_t is the mass of the biomass sample at a particular time, while α_f is the mass of biomass at the end of the pyrolysis reaction. By combining the above equations, the obtained equation is expressed as:

$$\frac{dx}{dt} = k_0 e^{-\left(\frac{E}{RT}\right)} (1-x)^n \quad (9)$$

δ is the heating rate. Heating rate (δ) can be defined as:

$$\delta = \frac{dT}{dt} = \frac{dT}{dx} \times \frac{dx}{dt} \quad (10)$$

now solving the eqn (5)–(10), the final expression can be written as

$$g(\kappa) = \int_0^x \frac{dx}{f(x)} = \int_0^T \frac{A}{\delta} e^{-(E/RT)} dT \quad (11)$$

$$g(\kappa) = \frac{AE}{\delta R} \int_0^x u^{-2} e^{-u} du = \frac{AE}{\delta R} p(x) \quad (12)$$

where $g(\kappa)$ represents integral conversion and $x = \frac{E}{RT}$. However, $p(x)$ has no exact solution; therefore, it can be solved by the numerical approximation method. $p(x)$ is varied with respect to the type of approximation selected for simplifying.

2.5.1. Kissinger–Akahira–Sunose (KAS). The Kissinger–Akahira–Sunose (KAS) method is a model-free (isoconversional) approach used to determine activation energy. By applying the standard approximation to the temperature integral in eqn (11) and simplifying:

$$\ln\left(\frac{\delta}{T^2}\right) = \ln\left[\frac{AE}{R_g(x)}\right] - \frac{E}{RT} \quad (13)$$

2.5.2. Ozawa–Flynn–Wall (OFW). The Ozawa–Flynn–Wall (OFW) method is a model-free approach used to estimate the kinetic parameter (activation energy) of a material. It applies Doyle's approximation and is expressed as:

$$\ln(\delta) = \ln\left[\frac{AE}{R_g(x)}\right] - 2.315 - 0.457\frac{E}{RT} \quad (14)$$

2.5.3. Distributed activation energy model (DAEM). Distributed Activation Energy Model (DAEM), originally proposed by Vand (1943) for analysing complex reactions in pyrolysis and fossil fuel combustion, was later adapted to estimate kinetic parameters of various biomass fuels and to better understand their reaction mechanisms.[23] This model has proven to be a robust tool for interpreting biomass pyrolysis kinetics and shows strong agreement with experimental results, particularly at low heating rates.[23] The model can be represented as:

$$1 - \frac{V}{V_t} = \int_0^\infty \exp\left(-A\int_0^t e^{-\left(\frac{E}{RT}\right)} dt\right) \int E dE \quad (15)$$

where V represents the effective volatile content and V_t represents the amount of volatile content at time t, A is a pre-exponential factor, and $\int(E)$ represents the distribution curve of activation energy. Further, the simplified method of the DAEM model is as follows:

$$\frac{V}{V_t} \cong 1 - \int_{E_s}^{\infty} (E)\mathrm{d}E = \int_{0}^{E_s} (E)\mathrm{d}E \tag{16}$$

Furthermore, a simplified DAEM model regarding the Arrhenius equation is given as:

$$\ln\left(\frac{\delta}{T^2}\right) = \ln\left(\frac{AR}{E}\right) + 0.6075 - \frac{E}{RT} \tag{17}$$

2.5.4. Vyazovkin model (VM). The Vyazovkin method provides more accurate estimates of activation energy compared to other model-free approaches, such as Flynn–Wall–Ozawa (FWO) and Kissinger–Akahira–Sunose (KAS), which rely on analytical approximations of the temperature integral, $g(\alpha)$.[24,25] The apparent activation energy for both biomasses is determined by minimising the following objective function[24,25] in MATLAB at each progressive conversion step.

$$\Phi(E_\alpha) = \sum_{i=1}^{n} \sum_{j\neq 1}^{n} \frac{I(E_\alpha, T_{\alpha,i})\delta_i}{I(E_\alpha, T_{\alpha,j})\delta_i} \tag{18}$$

The temperature integral is given as:

$$I(E_\alpha,\ T_\alpha) = \int_{T_{\alpha-\Delta\alpha}}^{T_\alpha} \exp\left(\frac{-E_\alpha}{RT}\right)\mathrm{d}T \tag{19}$$

Here, n, T, δ, R, A, and E represent the reaction order, absolute temperature (K), heating rate (°C min^{-1}), gas constant (J mol^{-1} K^{-1}), pre-exponential factor (min^{-1}), and activation energy (kJ mol^{-1}), respectively.

2.5.5. Starink method. The Starink model is a non-isothermal, model-free approach that differs slightly from the Kissinger–Akahira–Sunose (KAS) and Ozawa–Flynn–Wall (OFW) methods. Studies have shown that it provides higher accuracy in determining activation energy compared to KAS, OFW, and the Friedman methods.[26] Although Ozawa's method is roughly one order of magnitude less precise than Kissinger's, the Kissinger method yields an error margin of about 0.05%, while Starink method provides results that are up to five times more accurate.[27] The equation derived from its approximation can be expressed as:

$$\ln\left(\frac{\delta}{T^{1.8}}\right) = C_s - 1.0037\frac{E}{RT} \tag{20}$$

2.5.6. Coats-Redfern method. The Coats-Redfern model is a widely applied model-free approach for determining the reaction order and pre-exponential factor.[28] Activation energy, order of reaction and pre-exponential factor of DDGS were determined at a heating rate of 10 °C min^{-1}. Considering the reaction order (n), the rate of reaction can be expressed as:

$$\ln\left\{\frac{1-(1-x)^{1-n}}{T^2(1-n)}\right\} = \ln\left\{\frac{AR}{\delta E}\right\} - \frac{E}{RT}\ (\text{for}\quad n\neq 1) \tag{21}$$

$$\ln\left\{\frac{-\ln(1-x)}{T^2}\right\} = \ln\left\{\frac{AR}{\delta E}\right\} - \frac{E}{RT}\ (\text{for}\ n=1) \tag{22}$$

2.6. Thermodynamic analysis

Thermodynamic factors, namely Gibbs free energy (ΔG), Enthalpy (ΔH), and change in Entropy (ΔS), were evaluated as follows:

$$\Delta H = E - RT_m \tag{23}$$

$$\Delta G = E + R \times T_m \times \ln\left(\frac{K_B T_m}{hA}\right) \tag{24}$$

$$\Delta S = \frac{\Delta H - \Delta G}{T_m} \tag{25}$$

where A is the frequency factor (s^{-1}), T_m is peak decay temperature in (K), K_B is Boltzmann constant, and h is Planck constant (6.626×10^{-34}).

3. Results and discussions

3.1. Physicochemical characterisation of feedstock

The physical and chemical analysis of DDGS is listed in Table 2 and compared with other reported studies, such as corn cob, corn stover, Cotton stalk, and sorghum stalk.[29] The proximate, ultimate, biochemical, and fuel property analyses of DDGS in comparison with corn cob, corn stover, cotton stalk, and sorghum stalk reveal significant insights into its potential as a renewable energy resource. DDGS exhibits a very low moisture content (1.86%) compared to the other biomass (8.30–10.20%) in Table 2, which is highly advantageous for thermochemical conversion processes like pyrolysis and gasification since it minimises the need for drying and enhances thermal efficiency.[30] Furthermore, volatile matter (84.80%) of DDGS is considerably higher than that of the other feedstocks (66–80%), demonstrating that DDGS release a higher fraction of combustible gases during thermal decomposition, which supports rapid ignition and improved hot vapour yield.[31] The ash content (4.16%) of DDGS is moderate and lower than that of corn stover (11.10%) and sorghum stalk (8.80%), but slightly higher than cotton stalk (3.50%). The alternation in the proximate value arises due to the difference in the biochemical composition of biomass (Table 2). It was established that high ash content generally leads to operational problems during pyrolysis, like slagging, fouling, and reduced thermal efficiency.[32] The relatively lower ash content of DDGS supports its suitability as a clean-burning biomass fuel over the reported biomass in Table 2. The fixed carbon content (9.18%) of DDGS lies between that of corn cob (4.20%) and cotton stalk (16.60%), suggesting that while it may not retain as much solid char as cotton stalk, it provides a balance between volatile-driven gas production and solid residue formation.

The ultimate analysis highlights the uniqueness of DDGS as a biofuel. The carbon content (48.10%) is slightly higher than that of the other biomass (44.20–46.80%), which directly contributes to its higher energy density and calorific value.[33] Similarly, the hydrogen content (6.93%) is also comparatively higher than that of other biomass (Table 2), which improves

Table 2 Physicochemical characterisation of DDGC and comparison with the studied biomass

Analysis (%)	DDGS	Corn cob (CC)[29]	Corn stover (CRS)[29]	Cotton stalk (CS)[29]	Sorghum stalk (SS)[29]
Proximate analysis (wt%) dry basis					
Moisture content	1.86 ± 0.66	10.20	8.30	8.90	8.70
Volatile matter	84.80 ± 0.35	80.00	73.00	71.00	66.00
Ash content	4.16 ± 0.17	5.70	11.10	3.50	8.80
Fixed carbon	9.18	4.20	7.90	16.60	16.50
Elemental analysis (wt%) dry basis					
C	48.10	44.20	45.70	46.80	44.40
H	6.93	5.90	6.30	6.40	6.20
O	40.32	44.20	45.70	46.80	44.40
N	4.65	0.40	0.40	0.30	0.50
S	0	0.08	0.50	0.20	0.90
H/C	1.72				
O/C	0.62				
Heating value (MJ kg^{-1})	19.42	13.30	17.90	19.20	17.10
Bulk density (kg m^{-3})	471.21	—			
CrI (%)	54.65	43.00	56.00	56.00	55.00
Biochemical analysis (wt%)					
Cellulose	21.00	32.20	28.30	39.40	35.40
Hemicellulose	7.56	29.00	16.40	19.20	17.40
Lignin	30.01	18.40	23.80	24.80	21.30

fuel reactivity and enhances flame stability.[33] Further, the oxygen content (40.32%) in DDGS is lower than in the other biomass (44.20–46.80%), which is favourable because lower oxygen in the fuel leads to higher heating values and better combustion efficiency.[34] A distinguishing feature of DDGS is its significantly higher nitrogen content (4.65%) compared to the others (0.30–0.50%), which can pose challenges by contributing to NO_x emissions during combustion. However, it may also act beneficially in catalytic or nutrient recycling contexts when used for biochar production.[35] The sulphur is absent in DDGS compared with other biomass, which contains sulphur up to 0.9%. This absence of sulphur makes DDGS environmentally friendly and reduces the formation of SO_x-related emissions and corrosion problems in boilers.[36] Two important measures of biomass quality for pyrolysis are the H/C and O/C ratios. Higher H/C ratios improve combustion efficiency, fuel reactivity, and volatile release, but lower O/C ratios imply less oxygen, which results in higher heating values, better stability, and a higher output of bio-oil with less oxygenated molecules. The atomic ratios (H/C = 1.72 and O/C = 0.62) support its superior fuel quality, since the high H/C ratio improves combustion efficiency, while the moderate O/C ratio signifies a balance between reactivity and stability.[37] The HHV refers to the total energy released upon full combustion of a fuel and has a direct impact on process performance and economics. It is a crucial metric for assessing fuel efficiency, energy density, and appropriateness for power generation, heating, and biofuel applications. The higher heating value (HHV) of DDGS (19.42 MJ kg^{-1}) surpasses that of corn cob (13.30 MJ kg^{-1}), corn stover (17.90 MJ kg^{-1}), and sorghum stalk (17.10 MJ kg^{-1}), and is approximately equal to that of cotton stalk (19.20 MJ kg^{-1}), demonstrating that DDGS is an excellent energy-dense biomass feedstock.[38] The bulk density of biomass directly affects storage, handling, and transportation efficiency. Higher bulk density reduces logistic costs, improves feeding rates in reactors, and enhances energy density per unit volume, making biomass utilisation more practical and economical for large-scale bioenergy applications. The bulk density (471.21 kg m^{-3}) of DDGS is found to be significant, which adds an advantage for storage, handling, and transportation, reducing logistical costs compared to other loose biomasses. The crystallinity index (CrI) of DDGS (54.65%) is higher than that of corn cob (43%) but comparable to other biomass (55–56%), suggesting moderate crystalline cellulose content, which can influence thermal decomposition and enzymatic hydrolysis behaviour. The biochemical analysis highlights significant differences in composition between DDGS and other feedstocks. DDGS has relatively lower cellulose (21%) compared to corn stover (39.40%) and cotton stalk (35.40%), suggesting reduced potential for fermentable sugar recovery.[39] However, its lignin content (30.01%) is considerably higher than that of others (18.40–24.80%), which may enhance energy density and char yield but also makes enzymatic hydrolysis more difficult. Hemicellulose was found to be 7.56% which is much lower than in other biomass (16.40–29%), indicating easier decomposition at lower temperatures.[39] The physicochemical results of DDGS possess numerous favourable characteristics for bioenergy production, such as lower moisture, higher volatile matter, moderate ash, higher carbon and hydrogen, absence of sulphur, and greater HHV. The higher bulk density further adds logistical and storage advantages, while the biochemical composition supports rapid thermal breakdown due to abundant hemicellulose. The potential concerns include its higher nitrogen content, which can add positive value if the application is for biochar production.

3.2. Mineral and metal content analysis

The mineral and metal analysis provides valuable insight into its chemical composition and its potential behaviour during thermal conversion processes. The metal content of DDGS ash is listed in Table 3. The results reveal that phosphorus pentoxide (P_2O_5) is the dominant mineral component 38.41%, followed by potassium oxide (K_2O) 32.12% and calcium oxide (CaO) at 9.04%, while other oxides such as magnesium oxide (6.02%), sodium oxide (5.72%), sulphur trioxide (4.87%), and silica (2.56%) are present in moderate to lower amounts. Trace components include alumina (0.24%), ferric oxide (0.33%), and manganese oxide (0.69%). The high concentration of P_2O_5 indicates that the sample is rich in phosphorus-based compounds, which may be advantageous in terms of agricultural reuse as a fertiliser, but can cause slagging and fouling in thermochemical processes due to the formation of sticky phosphates with alkali metals.[32] Furthermore, the significant presence of K_2O (32.12%) intensifies the risk of ash-related operational challenges, as potassium is highly reactive and promotes the formation of low-melting eutectics with silica and phosphorus. The high proportions of P_2O_5 (38.41%) and K_2O (32.12%) in DDGS ash strongly influence pyrolysis kinetics by altering reaction pathways and apparent activation energy. Alkali metals like K catalyze cellulose and hemicellulose decomposition, lowering activation energy in early stages and enhancing gas yield, while phosphorus can interact with alkalis to form stable phosphates that suppress volatilization and increase char retention. These minerals thus create dual effects: catalytic acceleration of devolatilization at lower temperatures and inhibition through slagging or phosphate formation at higher stages. The CaO content (9.04%) is important since calcium often acts as a fluxing agent that lowers the melting point of ash, enhancing slagging tendency.[40] However, it can also provide catalytic effects that promote devolatilization and char gasification.[40] The MgO content (6.02%) contributes to basicity and may partially neutralise acidic oxides, stabilising ash behaviour, though at lower levels than CaO.[41] Sodium oxide (5.72%) in combination with potassium significantly increases total alkali content (37.84%), reinforcing the risk of alkali-related corrosion and agglomeration during combustion and gasification. Further, the presence of SO_3 (4.87%) may lead to sulfation reactions, particularly with alkali metals, forming alkali sulphates, which further exacerbate fouling and deposition on reactor surfaces.[32] Silica (2.56%) and alumina (0.24%) are relatively lower, which reduces the acidic buffering capacity of the ash and makes it more prone to alkali-driven melting.[32] The base-to-acid ratio (B/A) is 1.43, which is slightly above the conventional risk threshold of 1, indicating a system biased toward basic oxides and therefore a higher probability of slagging under combustion/gasification conditions. This aligns with the chemistry described above and reinforces the need for ash-management strategies. The alkali index (AI) of 0.81 kg GJ^{-1} indicates a substantial alkali loading per unit energy. The values of this magnitude often correlate with noticeable fouling unless mitigations (fuel blending, additives, or leaching) are applied, especially in grate or fluidised-bed systems with hot convective surfaces.[42] Calcium and magnesium play a nuanced role and can catalyse char gasification and secondary cracking, potentially improving gas quality.[43] The sulphur trioxide fraction (4.87%) favours formation of alkali sulphates (K_2SO_4, Na_2SO_4), which are sticky in the 600–800 °C range and contribute to deposit growth and tube corrosion. This risk is magnified by the high pool of K and Na available to sulphate, highlighting the importance of temperature zoning and surface cleaning regimes in boiler operation.[44] Similarly, the iron/calcium (I/C) ratio of DDGS ash was found to be 0.036, which highlights calcium dominance over iron, suggesting that fluxing and melting behaviour will be governed mainly by calcium rather than iron.[32] Total alkali in ash (mainly K and Na) plays a catalytic role during biomass pyrolysis, accelerating cellulose and hemicellulose decomposition, enhancing gas yield, and promoting tar cracking. However, excessive alkalis lower ash fusion temperatures, leading to slagging, fouling, and operational issues, making alkali content a critical factor in feedstock suitability.[42] Minerals and metals play a crucial role in biomass pyrolysis by influencing reaction pathways, product distribution, and ash behaviour. Alkali metals like K and Na catalyse cellulose and hemicellulose decomposition, enhancing gas yield but promoting char reactivity and tar cracking.[42] Calcium and magnesium act as catalysts for secondary reactions, improving bio-oil quality while reducing tar.[41] However, high alkali and alkaline earth content can lower ash melting points, leading to slagging and fouling issues. Finally, phosphorus contributes to nutrient-rich biochar but can form problematic phosphates.[42,45]

Table 3 Mineral and metal composition analysis along with slagging and fouling indices

Mineral	Composition (%, db)
Al_2O_3	0.24
CaO	9.04
Fe_2O_3	0.33
K_2O	32.12
MgO	6.02
Mn_3O_4	0.69
Na_2O	5.72
P_2O_5	38.41
SO_3	4.87
SiO_2	2.56
Total	100
Base-to-acid ratio	1.43
Alkali index (kg GJ^{-1})	0.81
Iron calcium ratio	0.036
Total alkali	37.84

3.3. Thermal analysis

The thermal decomposition profile of DDGS at different heating rates (10, 20 and 30 °C min) was presented in Fig. 1. The TGA profile of DDGS depicts a three-stage devolatilization pathway (drying stage (30–150 °C), active pyrolysis stage (150–600 °C) and char formation stage (>600 °C)) governed by biomass

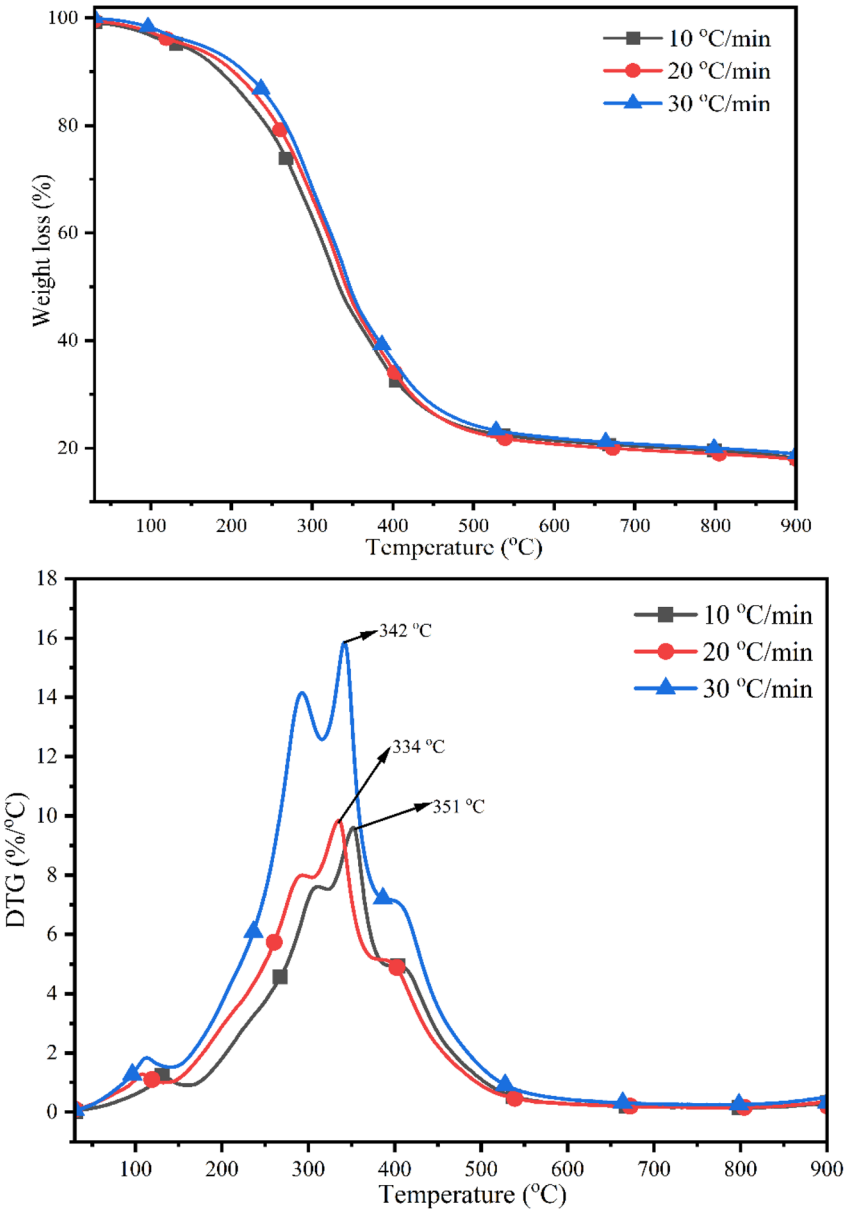

Fig. 1 Thermal decomposition profile of DDGS at 10, 20 and 30 °C min.

heterogeneity and heating-rate effects. A small mass loss below 150 °C was noticed, which reflects decomposition of higher volatile matter and moisture content. Its modest magnitude is consistent with a lower inherent moisture content and confirms that subsequent weight loss is dominated by chemical decomposition rather than drying. Kumar *et al.* (2020) and Bhardwaj *et al.* (2021) also reported similar results for banana trunk biomass, printing paper (AP), filter paper (FP), newspaper (NP), writing paper (WP), and reed pith (RP).[46,47] The principal mass loss occurs within 200–420 °C, where hemicellulose and cellulose depolymerise and deposit volatiles. This is mirrored in the DTG traces by a shoulder at lower temperature (typical of hemicellulose, 220–300 °C), followed by a sharp dominant peak attributable to cellulose depolymerisation and levoglucosan pathways.[48] The DTG thermograph indicate peak temperatures rising from 351 °C at 10 °C min^{-1}, 334 °C at 20 °C min^{-1} and 342 °C at 30 °C min^{-1}, respectively. The trend arose due to the fact that as the heating rate increases, intraparticle thermal gradients intensify and the sample reaches the same conversion at a higher apparent temperature (thermal lag), shifting DTG maxima rightward and increasing peak height (greater instantaneous reaction rate).[46] Simultaneously, the peak broadening at higher rates signals distributed activation energies and overlapping reactions of different biopolymers; sharper peaks at the highest rate reflect reaction-controlled regimes briefly outpacing heat removal.[47] The mass loss of DDGS decreased above 600 °C due to lignin degradation, with the TG curves converging to a residual fixed carbon fraction of roughly 18–20 wt%.[49] The sustained DTG signal after 600 °C indicates the high thermal stability of lignin's aromatic framework. The extended, low-

intensity decomposition across a wide temperature interval governs the formation and characteristics of the char.[49] At high temperature, it suggests the inorganic fraction is thermally stable and that the final solid yield is relatively insensitive to heating rate. Mechanistically, higher heating rates favour primary volatilisation over secondary cracking/condensation equilibria because vapours depart faster from hot zones; this tends to increase the DTG peak intensity and, in larger-scale reactors, translates into higher bio-oil precursors and less secondary char if vapour residence is short.[47] Conversely, the lower heating rates provide more time for *in situ* tar cracking and crosslinking, producing slightly more char and shifting volatiles toward non-condensable gases.[47] The systematic peak shift with increasing heating rate suggests that iso-conversional kinetic analysis would yield conversion-dependent activation energies, reflecting the complex, multi-step nature of biomass pyrolysis. Therefore, deriving a single global activation energy from one heating rate is insufficient and may lead to misinterpretation of the underlying reaction mechanisms.[50] The temperature span of rapid mass loss defines an optimal pyrolysis window (300–400 °C) for maximising volatile release while limiting excessive secondary degradation, and the observed residue fraction indicates the char potential and informs reactor solids handling. The presence of distinct hemicellulose and cellulose peaks in the DTG profile indicates that the feedstock retains a substantial fraction of polysaccharides, which decompose in their characteristic temperature ranges. This clear separation suggests that mineral-induced catalytic effects are not dominant, allowing the natural decomposition behaviour of the biopolymers to be expressed. Stronger mineral catalysis from alkali and alkaline earth metals would cause a clear leftward shift of the decomposition peaks and broader shoulders at lower temperatures, reflecting enhanced alkali-driven fragmentation. Thus, the observed thermal pattern highlights that the mineral fraction exerts only limited catalytic influence on early-stage pyrolysis.[51] He *et al.* (2025) revealed distinct decomposition behaviours for *Chlorella vulgaris* (CV) and polyvinyl chloride (PVC). CV showed five stages of weight loss, starting with dehydration at 150–245 °C, followed by rapid carbohydrate decomposition between 245-300 °C, protein degradation from 300–386 °C, and lipid decomposition with a total mass loss exceeding 60%. PVC decomposes in two main stages: dechlorination at 250–370 °C with 65 wt% loss, followed by carbon-chain breakdown from 370–560 °C. For mixed samples, synergistic effects were observed between 220-390 °C.[52] Wang *et al.* (2024) revealed that Chlorella vulgaris (CV) decomposed in five stages: moisture loss (150–245 °C, 7%), carbohydrates (peak 295 °C), proteins (peak 340 °C), lipids (8%), and char decomposition (>500 °C). Polyethylene (PE) showed a single sharp peak between 423–532 °C. Furthermore, the highest synergistic effect occurred in stage five, with ΔTG 4%, especially at a 3 : 1 CV : PE ratio.[53] Furthermore, the heating-rate sensitivity highlights the need for tight control of particle size and heat flux at larger-scale trials. Larger particles or insufficient heat transfer would broaden conversion zones and demand longer residence times to reach the same extent of devolatilization.[47]

3.4. FTIR analysis of DDGS

FTIR spectrum of DDGS shows clear signals that indicate the presence of polysaccharides, proteins, aromatics, hydroxyethyl group, *etc.* The wavenumber against transmission spectra was listed in Fig. 2. The broad IR band around 3280 cm^{-1} comes from O–H stretching in water and the hydroxyl groups of cellulose/hemicellulose, and it also overlaps with N–H stretching from protein. Its broad shape and position show strong hydrogen bonding.[54] Furthermore, the pair of bands at 2925 cm^{-1} (asymmetric) and 2850 cm^{-1} (symmetric) is the typical aliphatic C–H stretching vibrations of CH_2/CH_3 groups and points to residual fats/oils and aliphatic side chains in proteins.[55] A relatively strong and sharp band at 1742 cm^{-1} corresponds to unconjugated C=O stretching (ester or carbonyl groups) and is attributed to acetyl groups of hemicellulose, and small amounts of free organic acids.[56] The IR bands at 1614 and 1525 cm^{-1} are diagnostic of aromatic C=C stretch vibrations, respectively. The IR band 1614 cm^{-1} likely contains contributions from aromatic skeletal vibrations of lignin and conjugated C=O, while 1525 cm^{-1} is consistent with N–H bending/C–N stretching from protein content in DDGS.[57] The IR band 1371 cm^{-1} is typical of C–H bending (methyl/methylene deformation) and indicates lignin methoxyl.[57] The band at 1221 cm^{-1} commonly corresponds to C–O stretching of aryl-O or C–O–C vibrations in lignin (guaiacyl/syringyl structures) and ester C–O stretches (supporting the 1742 cm^{-1}), which signals the presence of lignin-related functional groups and ester linkages.[58] The strong absorption at 1030 cm^{-1} is characteristic of C–O stretching and C–O–C vibrations in cellulose and hemicellulose (polysaccharide fingerprint region), and its intensity underlines that carbohydrates are a dominant fraction of the DDGS matrix.[59] Finally, the small peaks at 525 and 473 cm^{-1} fall in the inorganic region and are most plausibly due to metal oxygen lattice vibrations or phosphate/silicate related stretches.[56] Overall, the relative intensities and positions indicate a composite material. The strong polysaccharide bands (1030 and 1221 cm^{-1}) confirm cellulose/hemicellulose, the amide and N–H features (1525 and 3280 cm^{-1}) reflect significant protein

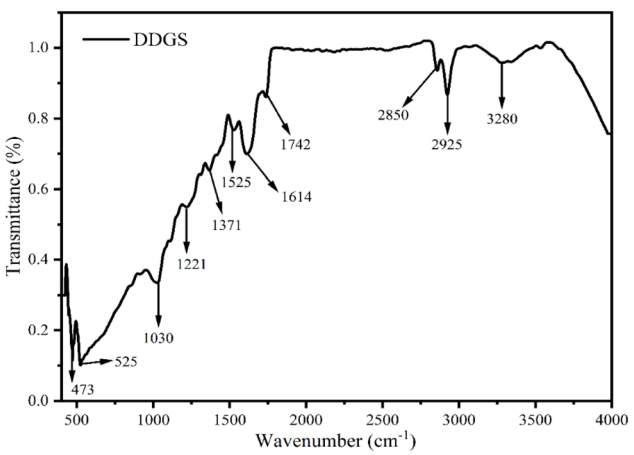

Fig. 2 FTIR analysis of DDGS.

residuals typical of DDGS, the C=O (1742 cm^{-1}) and aliphatic CH stretches (2850 and 2925 cm^{-1}) show residual esters, and the low-frequency modes reveal inorganic ash.

3.5. Burnout temperature

The burnout temperature is the point at which nearly all the fuel (gases and solid carbon) has burned up during combustion, leaving mostly ash. Therefore, understanding this temperature aids in enhancing energy efficiency and assessing the fuel burn efficiently. The number of variables, including the biomass types, residence time, heating rate, and the use of catalysts, affects the burnout temperature. Since biochar is a good material for soil improvement and carbon storage, the total burnout is not desired in pyrolysis procedures used to produce biochar. Researchers frequently examine and contrast the pyrolysis and combustion behaviour of biomass using the idea of burnout temperature (El-Sayed & Mostafa, 2014; Mishra & Mohanty, 2018b). Further, Mishra *et al.* (2024) observed that burnout temperature is strongly influenced by the heating rate. They reported that by increasing the heating rate from 10–50 °C min, the burnout temperature changed to 598, 587, and 566 °C for neem seeds, and to 610, 542, and 519 °C for waste nitrile gloves, respectively.[60] From Fig. 3, it was noticed that by increasing heating rates from 10–30 °C min, the burnout temperature increased to 637, 669 and 680 °C, respectively. This trend highlights the effect of heating rate on the thermal behaviour of biomass during pyrolysis and combustion. At higher heating rates, the material undergoes more rapid decomposition, breaking down into volatile gases and char in a shorter time. This quick release of volatiles alters the kinetics of the process and shifts the onset and completion of char combustion. Moreover, faster heating improves heat and mass transfer within the biomass particles, which reduces the residence time at intermediate temperatures and accelerates the overall reaction. As a result, the burnout temperature is reached more quickly, reflecting faster thermal decomposition and combustion reactions. However, it is important to note that while higher heating rates increase reaction speed, they may also reduce the completeness of combustion due to shorter residence times for volatiles.

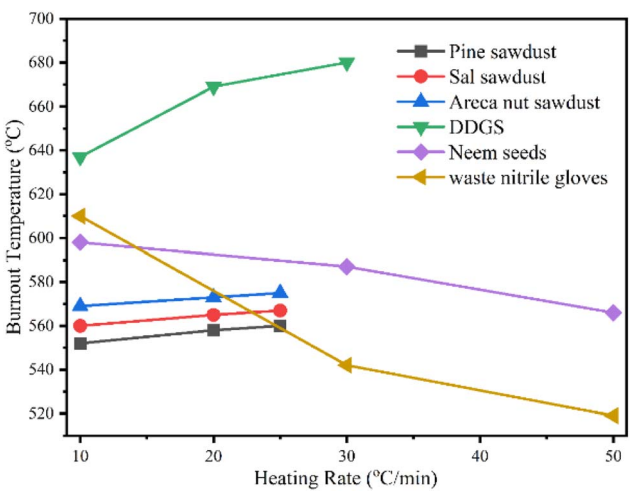

Fig. 3 Burnout temperature of DDGS along with pine, sal, areca nut sawdust, need seeds and waste nitrile gloves.

3.6. Kinetic analysis

The kinetic analysis of DDGS pyrolysis using model-free approaches provides valuable insights into the complexity of its thermal decomposition and the reaction mechanisms governing volatile release, char formation, and gas evolution. The kinetic analysis of DDGC was evaluated as a function of conversion (α) using KAS, OFW, STM, DAEM, and VZM, and is listed in Table 4. From the results, it was noticed that DDGS pyrolysis is a multi-step process rather than a single-reaction process. Model fitting at higher conversion ($\alpha = 0.8$) exhibited weaker agreement, as reflected in the reduced correlation coefficient.[28] It was noticed that from the conversion value 0.1–0.3, the activation energy (140–160 kJ mol^{-1}, depending on the method) was found to be relatively lower due to decomposition of hemicellulose and early degradation of amorphous cellulose, indicating that these fractions require less energy to initiate devolatilization due to their less ordered structures and greater thermal reactivity.[47] A large variation in activation energy was found for activation energy across conversion values, which can make the calculation of the average complicated. A similar observation was made by Kumar *et al.* (2019)[61] and Damartzis *et al.* (2011).[28] Furthermore, conversion value 0.3–0.6 is dominated by the depolymerisation and volatilisation of crystalline cellulose; thus, activation energy values increase significantly from 180–345 kJ mol^{-1}, reflecting the higher bond dissociation energy and more ordered crystalline domains of cellulose, which resist thermal breakdown.[62] Further, at a higher conversion range (0.6–0.8), the activation energy trend becomes more variable due to the overlapping decomposition of lignin and the formation of secondary char. The activation energy varies from 345–525 kJ mol^{-1}, resulting from complex radical reactions, cross-linking, and condensation processes.[63] Kinetic results showed a close agreement among KAS, OFW, and STM in terms of average activation energy trends, which provides reliability and consistency in the kinetic evaluation, although slight differences in absolute values arise from their mathematical approximations. Among all the selected models, DAEM and VZM provide lower activation energy (250.48 and 213.91 KJ mol^{-1}). DAEM and VZM yield lower activation energies because they better capture the multi-step nature of DDGS pyrolysis. DAEM averages reactions through a distribution, reducing overestimation from high-activation energy processes. In contrast, VZM, as a differential method, avoids errors in integral approximations, producing more realistic values compared to KAS, OFW, and STM. Activation energy is independent of the specific pyrolysis reaction mechanism and holds a physical significance that can be explained through Molecular Collision Theory (MCT).[64] According to this theory, during random pyrolysis, only certain molecular collisions acquire sufficient kinetic energy to disrupt existing bonds and initiate reactions. These activated collisions may temporarily break old bonds,

Table 4 Kinetic analysis of DDGS using KAS, OFW, STM, DAEM, VZ and CR models

Model name	Conversion value	Apparent activation energy (kJ mol^{-1})	Frequency factor (A, 1/min)	R^2	Equation
KAS					
	0.1	89.74	3.27583×10^{9}	0.9993	$y = -10795x + 12.623$
	0.2	117.74	3.56399×10^{11}	0.9998	$y = -14162x + 17.041$
	0.3	172.07	1.49838×10^{16}	0.9913	$y = -20697x + 27.308$
	0.4	220.34	9.14216×10^{19}	0.9697	$y = -26503x + 35.777$
	0.5	253.18	1.39385×10^{22}	0.9736	$y = -30453x + 40.665$
	0.6	334.84	1.70763×10^{28}	0.9634	$y = -40275x + 54.404$
	0.7	429.88	3.59821×10^{34}	0.9839	$y = -51706x + 68.715$
	0.8	514.12	4.80692×10^{38}	0.9794	$y = -61839x + 78.036$
Average	Total	266.49	6.009100×10^{37}		
OFW					
	0.1	97.84	6.26794×10^{15}	0.9994	$y = -11769x + 27.001$
	0.2	126.52	7.90336×10^{17}	0.9998	$y = -15218x + 31.581$
	0.3	181.32	3.61196×10^{22}	0.9922	$y = -21810x + 41.951$
	0.4	229.97	2.36687×10^{26}	0.9721	$y = -27661x + 50.501$
	0.5	263.17	3.86607×10^{28}	0.9755	$y = -31654x + 55.462$
	0.6	345.20	5.05340×10^{34}	0.9655	$y = -41521x + 69.274$
	0.7	440.79	1.17280×10^{41}	0.9847	$y = -53018x + 83.687$
	0.8	525.74	1.77589×10^{45}	0.9803	$y = -63236x + 93.136$
	Total	276.32	2.22000×10^{44}		
DAEM					
	0.1	105.39	3.84694×10^{9}	0.9999	$y = -12677x + 14.739$
	0.2	146.72	4.44128×10^{11}	0.9996	$y = -17648x + 22.622$
	0.3	188.29	1.63962×10^{16}	0.9996	$y = -22648x + 30.281$
	0.4	224.41	9.31084×10^{19}	0.9596	$y = -26992x + 36.433$
	0.5	243.30	1.33943×10^{22}	0.9693	$y = -29264x + 38.864$
	0.6	293.65	1.49758×10^{28}	0.9736	$y = -35321x + 47.282$
	0.7	401.34	3.35931×10^{34}	0.9899	$y = -48273x + 65.489$
	0.8	400.76	3.74703×10^{38}	0.9999	$y = -48204x + 62.166$
	Total	250.48	4.68421×10^{37}	0.9999	
STM					
	0.1	90.04	5.80605×10^{9}	0.9994	$y = -10831x + 13.192$
	0.2	118.09	6.39069×10^{11}	0.9998	$y = -14204x + 17.622$
	0.3	172.44	2.69529×10^{16}	0.9914	$y = -20741x + 27.893$
	0.4	220.72	1.65045×10^{20}	0.9698	$y = -26549x + 36.366$
	0.5	253.58	2.52349×10^{22}	0.9736	$y = -30501x + 41.257$
	0.6	335.25	3.09974×10^{28}	0.9635	$y = -40324x + 54.999$
	0.7	430.31	6.54984×10^{34}	0.9839	$y = -51758x + 69.313$
	0.8	514.59	8.80184×10^{38}	0.9794	$y = -61895x + 78.64$
	Total	266.88	1.10031×10^{38}		
VZM		Apparent activation energy (kJ mol^{-1})	Error		
	0.1	82.06	0.00017		
	0.2	95.77	0.00049		
	0.3	150.85	0.00015		
	0.4	197.97	0.00980		
	0.5	234.95	0.00112		
	0.6	263.29	0.00230		
	0.7	350.00	0.02301		
	0.8	336.44	0.00201		
	Total	213.91			

which are subsequently replaced by new bonds, leading to the formation of new molecules. Furthermore, the reactivity of a fuel governed by its activation energy plays a crucial role in pyrolysis and is highly relevant for the design and optimisation of pyrolysers.[65]

Fig. 4 illustrates the variation of activation energy with conversion value, showing that the apparent activation energy increases over conversion value 0.8. The pyrolysis behaviour of DDGS closely correlates with its biochemical composition, as hemicellulose, cellulose, and lignin decompose at different temperature ranges, directing the apparent activation energy across the conversion pathway. At the initial conversion stage (0.1–0.3), decomposition is primarily controlled by hemicellulose and cellulose, which contain branched, thermally

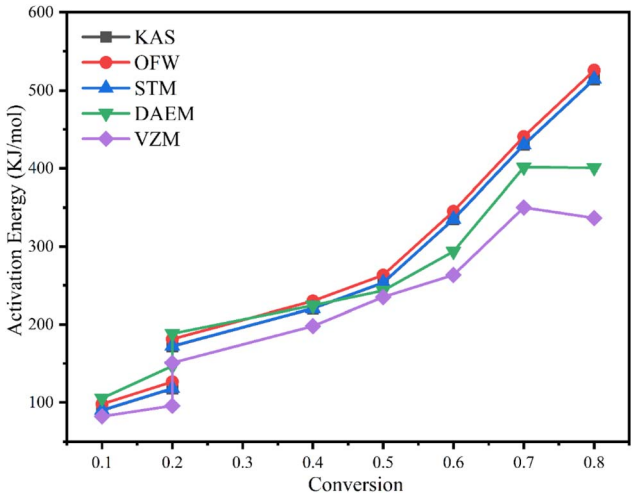

Fig. 4 Variation of apparent activation energy against conversion value.

labile structures with weaker glycosidic bonds.[66] Their lower thermal stability leads to relatively small activation energy values (Table 4), consistent with the early devolatilisation peak observed between 220-300 °C (DTG analysis). This stage facilitates rapid volatile release and easy ignition, supporting syngas and bio-oil production. In the intermediate stage (0.3–0.6), crystalline cellulose becomes the dominant fraction undergoing degradation. The lower cellulose (21%) and high lignin (30%) content of DDGS significantly affect its pyrolysis kinetics. Limited cellulose reduces the sharp mid-temperature depolymerisation peak, resulting in lower activation energy variation during 0.3–0.6 conversion. Owing to its ordered, hydrogen-bonded crystalline domains, cellulose requires significantly higher bond dissociation energies, reflected in a sharp increase in activation energy values (Table 4). This corresponds with the major DTG peak around 330–360 °C, indicating rapid depolymerisation and volatilisation. At higher conversions (0.6–0.8), lignin decomposition dominates (in the passive stage). Lignin is a highly aromatic, cross-linked structure that undergoes a broad, heterogeneous breakdown through radical reactions, condensation, and char stabilisation.[66] This results in highly variable and elevated activation energy values (Table 4), along with sustained mass loss beyond 600 °C. The persistence of high activation energy at this stage indicates the recalcitrance of lignin-derived char, which contributes to the formation of stable carbon residues suitable for biochar applications. The higher lignin content extends decomposition over a broad temperature range, producing elevated and variable activation energies between 0.6 and 0.8 conversion. This explains the sustained mass loss and high char yield at higher temperatures, reflecting lignin's recalcitrant aromatic network. Thus, DDGS exhibits higher average activation energy and slower thermal degradation than cellulose-rich feedstocks, requiring greater energy input for complete conversion and favouring char-rich products. Overall, the progressive increase in activation energy with conversion aligns with the sequential degradation of hemicellulose, cellulose, and lignin, confirming the multi-step nature of DDGS pyrolysis. Further, the curve fitting of KAS, OFW, STM and DAEM models is also listed in Fig. 5. However, there is a variation in activation energy among the selected models due to mathematical models, biochemical composition, and the use of different approximation methods.[46]

The pre-exponential factors (A) derived from these models further confirm the multistep nature of the process. Higher frequency factors are observed in cellulose decomposition, consistent with rapid devolatilization, while lower values in lignin degradation indicate slow, heterogeneous reactions. These findings logically align with the proximate and biochemical composition of DDGS (Table 2). The higher volatile matter supports rapid devolatilization in the mid-temperature region, while its relatively high lignin content sustains prolonged decomposition and char formation over a broader temperature range. The variation in activation energy with conversion also highlights the catalytic influence of inherent alkali and alkaline earth metals present in DDGS ash, which may promote fragmentation and tar cracking at lower temperatures. However, the overall kinetic behaviour still reflects the dominant role of macromolecular structure.[67] Importantly, the dependence of activation energy on conversion emphasises that assigning a single global kinetic parameter to DDGS pyrolysis would be misleading. Such an approach would oversimplify the process and ignore the distinct contributions of hemicellulose, cellulose, and lignin fractions.[67] The model-free methods provide a more realistic representation of the energy barriers across the conversion pathway, making them suitable for predictive modelling and reactor design. Logically, the relatively moderate activation energy values in the early stage (0.1–0.03) suggest that DDGS can be easily ignited and rapidly decomposed to produce volatiles, favouring bio-oil and syngas production under controlled pyrolysis conditions. However, the higher activation energy values in the cellulose-dominated region necessitate optimised heating rates to ensure complete conversion.[63] In addition, the persistence of higher activation energy at later stages also indicates that lignin-derived char is more resistant, implying that DDGS could yield a stable biochar fraction suitable for carbon sequestration or soil amendment.[63] The kinetic analysis clearly demonstrates that DDGS pyrolysis follows a multi-step, overlapping reaction pathway strongly influenced by its biochemical composition. Hemicellulose contributes to lower activation energy during early decomposition, cellulose dominates mid-stage reactions with higher energy barriers, and lignin governs late-stage char stability. Model-free isoconversional methods effectively capture conversion-dependent kinetics, while model-fitting approaches provide mechanistic interpretations, together supporting a comprehensive understanding of its thermal behaviour.[63]

The Coats-Redfern (CR) model was applied at a single heating rate of 10 °C min. Unlike iso-conversional models, the kinetic parameters, such as activation energy and order of reaction, were estimated. The order of reaction does not have a direct physical meaning and is regarded as a fitting parameter.[28] The CR model was employed to estimate reaction order and corresponding activation energies using a trial-and-error method. The results showed activation energies of

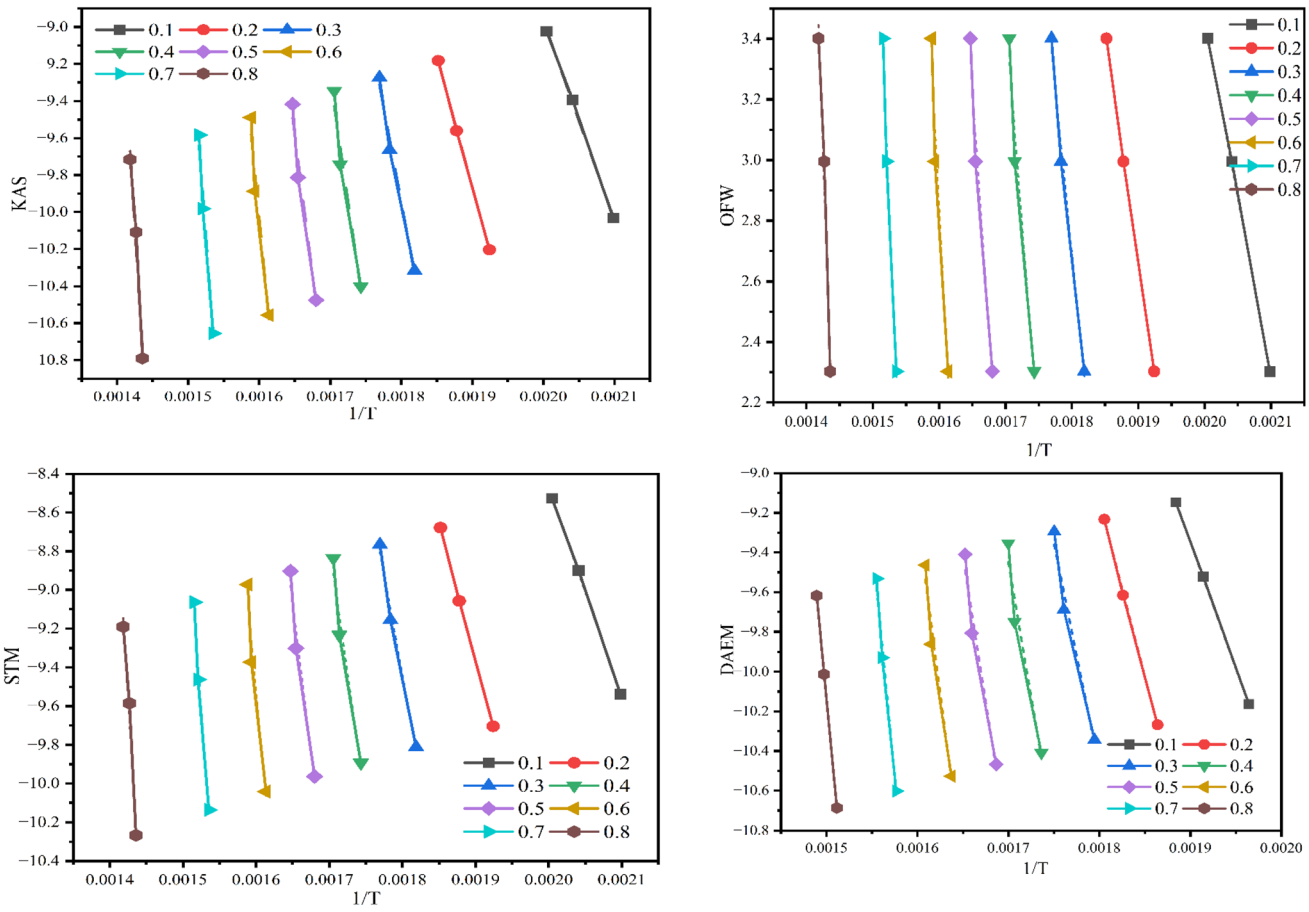

Fig. 5 Curve fitting of the KAS, OFW, STM and DAEM models.

36.32 kJ mol^{-1} and $R^2 = 0.9951$ at $n = 1$. Further, DDGS revealed 39.34 KJ mol^{-1} activation energy at $n = 2.1$. The results showing E_a of 36.32 kJ mol^{-1} at $n = 1$ with a high correlation ($R^2 = 0.9951$) and 39.34 kJ mol^{-1} at $n = 2.1$ indicate that DDGS pyrolysis does not follow a single-step mechanism but rather a multi-step, complex process. The slight increase in activation energy with a change in reaction order suggests that different components of DDGS, such as hemicellulose, cellulose, and lignin, decompose through overlapping pathways requiring different energy barriers. This behaviour highlights the heterogeneous nature of DDGS, where reaction order and activation energy vary with conversion, reflecting structural complexity and diverse thermal degradation mechanisms. Alkali metals such as K and Na act as strong catalysts that accelerate the decomposition of cellulose and hemicellulose by lowering their activation energies, thereby promoting volatile release and enhancing secondary cracking of tar into gases. This catalytic effect often explains the relatively lower E_a values observed in early conversion stages (0.1–0.3, our results supported the statement), where rapid hemicellulose breakdown occurs. Conversely, phosphorus, primarily present as P_2O_5, can react with alkalis to form stable phosphates, which reduce volatility and stabilise char, resulting in higher activation energies at advanced conversion stages dominated by lignin decomposition. CaO and MgO also contribute by facilitating secondary reactions, improving gas quality, and influencing char reactivity. Thus, the mineral composition of DDGS accelerates and inhibits reactions at different stages, producing a complex kinetic profile. Integrating these mineral effects into kinetic modelling can improve mechanistic understanding.

The activation energy obtained in the present study shows good agreement with values reported for switchgrass, *Cynodon dactylon*, *Lagerstroemia speciosa* seed hulls, Mustard straw, potato stalk, Sugarcane leaves, pine sawdust, sal sawdust, areca nut sawdust, and Siberian Fir Bark.[65,68–72] The kinetic analysis results demonstrate that the activation energy of DDGS and other reported biomass in Table 5 varies significantly depending on the applied model, highlighting the complexity of biomass decomposition. However, it is important to note that each biomass exhibits a distinct degradation temperature range, primarily influenced by its composition. Moreover, the activation energy is strongly affected by the type of feedstock, the applied kinetic model, and the pyrolysis operating conditions. The KAS and OFW methods yield closely comparable values (266.49 and 276.32 kJ mol^{-1}, respectively), suggesting reliable consistency between these model-free approaches. The DAEM method produces a slightly lower activation energy (250.48 kJ mol^{-1}), which reflects its ability to account for

Table 5 Comparison of average apparent activation energy against conversion value using model-free methods

Biomass	Heating rate (°C min^{-1})	KAS (kJ mol^{-1})	OFW (kJ mol^{-1})	DAEM (kJ mol^{-1})	STM (kJ mol^{-1})	VZM (kJ mol^{-1})	CR (kJ mol^{-1}) $n = 1$ E	CR (kJ mol^{-1}) $n \neq 1$ E	References
DDGS	10, 20 and 30	266.49	276.32	250.48	266.88	213.91	36.32	39.34 ($n = 2.1$)	Present study
Cynodon dactylon	10, 30 and 50	216.45	220.43	214.28		—	—	—	68
Lagerstroemia speciosa seed hulls	10, 15, 20, 30, and 40	154.35	164.00	—		141.93	—	—	69
Mustard straw	10, 15, 20, 30, and 40	201.80	202.19	—		202.12	—	—	70
potato stalk	10–30	122.79	125.99	—	—	122.85	—	—	73
Sugarcane leaves	5, 10, 15, 20, 30 and 40	226.75	226.97	—		215.11	—	—	71
Pine sawdust	5, 10, 15, 20 and 25	171.66	179.29	206.62		—	50.19	64.13	65
Sal sawdust	5, 10, 15, 20 and 25	148.44	156.58	171.63		—	43.89	57.97	
Areca nut husk	5, 10, 15, 20 and 25	171.24	179.47	160.45		—	52.90	63.41	
Siberian fir bark	2, 10 and 20	—	159	—	—	—	65	—	72

distributed reactions occurring during pyrolysis. In contrast, the STM method shows 266.88 kJ mol^{-1}, aligning well with KAS and OFW, further validating the reliability of the obtained values. Interestingly, the VZM model provides a much lower value (213.91 kJ mol^{-1}), which may be attributed to differences in mathematical assumptions regarding reaction mechanisms. The Coats-Redfern (CR) approach shows considerably lower energy barriers (36.32 kJ mol^{-1} for $n = 1$ and 39.34 kJ mol^{-1} for $n \neq 1$, $n = 2.1$), indicating its tendency to underestimate activation energy compared to iso-conversional methods. DDGS displays relatively higher activation energies compared with other biomasses reported in the literature, such as *Cynodon dactylon* (216.45–220.43 kJ mol^{-1}) and sugarcane leaves (226.75–226.97 kJ mol^{-1}), suggesting a stronger thermal stability and slower decomposition behaviour. These findings confirm that model selection greatly influences kinetic evaluation but consistently indicate that DDGS requires higher energy for thermal conversion, making it comparatively more resistant to degradation.

3.7. Thermodynamic analysis

The thermodynamic analysis of DDGS using KAS, OFW, STM, and DAEM provides a deeper understanding of the energy requirements, spontaneity, and molecular disorder associated with the thermal decomposition process. The thermodynamic analysis of DDGS using KAS, OFW, STM, and DAEM activation energy is listed in Table 6. Further, the observed variations across conversion stages reflect the complexity and multistep nature of biomass degradation. The enthalpy change (ΔH) values from all models indicate that pyrolysis is endothermic, requiring energy for bond breaking, with the energy demand increasing steadily as conversion rises from 0.1 to 0.8. For the KAS model, ΔH rises from 84.63 kJ mol^{-1} at $\alpha = 0.1$ to 509.01 kJ mol^{-1} at $\alpha = 0.8$, while in the OFW model it increases from 92.73 to 520.62 kJ mol^{-1}. Similarly, the STM model shows a rise from 84.93 to 509.48 kJ mol^{-1}, and the DAEM model from 100.28 to 395.65 kJ mol^{-1}. These results clearly demonstrate that

Table 6 Thermodynamic analysis of DDGS using the Activation energy obtained from the KAS, OFW, STM, and DAEM models[a]

Model name	Conversion	ΔH (kJ mol^{-1})	ΔG (kJ mol^{-1})	ΔS (J mol^{-1} k)
KAS	0.1	84.63	152.99	−111.13
	0.2	112.62	157.01	−72.14
	0.3	166.96	156.88	16.37
	0.4	215.23	160.58	88.83
	0.5	248.07	167.71	130.63
	0.6	329.73	177.67	247.18
	0.7	424.76	198.24	368.24
	0.8	509.01	233.90	447.22
Average		**261.38**	**175.62**	**139.40**
OFW	0.1	92.73	87.11	109.12
	0.2	121.40	91.05	49.34
	0.3	176.21	90.98	138.55
	0.4	224.85	94.68	211.61
	0.5	258.05	101.82	253.97
	0.6	340.09	111.82	371.06
	0.7	435.67	132.45	492.92
	0.8	520.62	168.17	572.95
Average		**271.21**	**109.76**	**262.44**
STM	0.1	84.93	150.36	−106.37
	0.2	112.97	154.36	−67.28
	0.3	167.32	154.25	21.25
	0.4	215.61	157.94	93.75
	0.5	248.47	165.07	135.56
	0.6	330.13	175.03	252.14
	0.7	425.20	195.61	373.22
	0.8	509.48	231.27	452.25
Average		**261.76**	**172.99**	**144.31**
DAEM	0.1	100.28	167.82	−109.79
	0.2	141.61	184.86	−70.31
	0.3	183.18	172.64	17.12
	0.4	219.29	164.55	88.99
	0.5	238.18	158.03	130.30
	0.6	288.54	137.16	246.09
	0.7	396.22	170.05	367.67
	0.8	395.65	121.81	445.15
Average		**245.37**	**159.61**	**139.40**

[a] Note: ΔH, ΔG are in kJ mol^{-1} and ΔS is in J mol^{-1}.K.

higher energy is required for the breakdown of more recalcitrant biomass components, such as crystalline cellulose and lignin, during the later stages of pyrolysis. This trend logically correlates with the biochemical composition of DDGS, where hemicellulose decomposes more easily at lower temperatures and conversions, while lignin contributes to stable structures that demand higher energy input for degradation at higher conversions. Gibbs free energy (ΔG) indicates the feasibility and spontaneity of the reaction. The results show consistently positive values across all models, ranging from about 87–233 kJ mol^{-1} for KAS, 87–168 kJ mol^{-1} for OFW, 150–231 kJ mol^{-1} for STM, and 121–184 kJ mol^{-1} for DAEM, signifying that the pyrolysis process is non-spontaneous and requires an external energy supply. The OFW model gives lower ΔG values (average 109.76 kJ mol^{-1}) compared to KAS (175.62 kJ mol^{-1}) and STM (172.99 kJ mol^{-1}), indicating that approximation methods influence the estimated thermodynamic barrier. However, all models confirm that DDGS pyrolysis needs external thermal energy to proceed. Our results are consistent with findings reported for cattle manure[74] and rubber wood.[75]

The entropy change (ΔS) values reveal further mechanistic insights, with negative values at low conversions for KAS, STM, and DAEM (−111.13, −106.37, and −109.79 J mol^{-1} K^{-1}, respectively, at $\alpha = 0.1$), indicating a transition to a more ordered activated complex during the initial stages due to the organised depolymerisation of hemicellulose and cellulose chains. However, as conversion value increases, ΔS values become positive and rise substantially, reaching 447.22 J mol^{-1} K^{-1} (KAS), 572.95 J mol^{-1} K^{-1} (OFW), 452.25 J mol^{-1} K^{-1} (STM), and 445.15 J mol^{-1} K^{-1} (DAEM) at conversion $\alpha = 0.2$–0.8, which implies increasing molecular randomness as lignin fragments and complex cross-linking reactions dominate, producing a greater diversity of volatile compounds and free radicals. The higher ΔS values in the OFW model (average 262.44 J mol^{-1} K^{-1}) compared to the others (KAS 139.40, STM 144.31, and DAEM 139.40 J mol^{-1} K^{-1}) suggest that this model captures greater disorder in the system, possibly due to its integral approximation method overestimating entropy changes at higher conversions. The obtained results have good agreement with the reported study by Aslan *et al.* (2018) for Medium Density Fiberboard (MDF). The thermodynamic study of DDG showed that it is an energy-demanding, non-spontaneous process where early-stage decomposition requires lower energy and involves more ordered transition states, while later stages require progressively higher energy and result in greater molecular disorder. The consistency among models in showing rising ΔH, positive ΔG, and the transition of ΔS from negative to positive reinforces the interpretation that DDGS pyrolysis follows a multistep pathway governed by the sequential breakdown of hemicellulose, cellulose, and lignin. These findings highlight that efficient utilisation of DDGS in thermochemical processes requires optimised heating strategies to supply sufficient energy for high-conversion stages. They also show that greater molecular randomness must be considered, as it affects product distribution. The variation in thermodynamic parameters between models further emphasises the importance of employing multiple approaches to capture the complex reality of biomass pyrolysis. OFW generally predicts higher entropy and lower Gibbs free energy, while KAS, STM, and DAEM offer more conservative estimates of system disorder and spontaneity.

The physical significance of thermodynamic parameters explaining the DDGS composition, which influences the pyrolysis process. The enthalpy change (ΔH) reflects the energy required to break chemical bonds. Lower ΔH at early stages corresponds to hemicellulose and amorphous cellulose decomposition, while higher ΔH at later stages arises from the stronger bonds in crystalline cellulose and lignin aromatic network.[76] Gibbs free energy (ΔG) signifies that pyrolysis is non-spontaneous and requires external energy, especially during cellulose depolymerisation and lignin fragmentation, aligning with the higher stability of these components. Entropy (ΔS) indicates structural changes: negative values at initial stages reflect ordered transition states during early chain scission, whereas positive values at advanced stages signify greater molecular disorder due to radical generation, cross-linking, and char formation from lignin. Overall, these parameters clarify that DDGS exhibits energy-intensive, multi-step kinetics and highlight the role of its lower cellulose and high lignin content in governing thermal behaviour.[76]

4. Conclusions

The present study provides a comprehensive kinetic and thermodynamic evaluation of DDGS pyrolysis using both model-free and model-fitting approaches. The results showed that the apparent activation energy (Ea) varies significantly with conversion, ranging from 82 to 525 kJ mol^{-1}, highlighting the multi-step nature of pyrolysis driven by the sequential decomposition of hemicellulose, cellulose, and lignin. Model-free methods such as KAS, OFW, STM, and VZM effectively captured the conversion-dependent kinetics, while the DAEM approach provided more realistic estimates for overlapping reactions. The Coats-Redfern model further supported this complexity, yielding reaction orders between 1.0 and 2.7 with corresponding activation energies ranging from 28.49 to 78.49 kJ mol^{-1}. Thermodynamic parameters revealed that DDGS pyrolysis is an endothermic and non-spontaneous process, as indicated by positive ΔG values (87–233 kJ mol^{-1}), with ΔH increasing up to 520 kJ mol^{-1} at higher conversions. Additionally, the transition of entropy (ΔS) from negative to positive indicates increasing molecular disorder as decomposition advances, especially during lignin degradation and char formation. Overall, the findings highlight that DDGS is a suitable but thermally demanding feedstock, and optimising heating conditions is crucial for efficient energy recovery. These insights contribute to reactor design, process modelling, and the sustainable valorisation of DDGS in bioenergy systems.

Author contributions

Gaurav Singh: data curation, investigation, visualisation, writing – original draft, Neeraj Kumar: data curation, visualisation, writing – original draft, editing original draft, and

supervision, Ranjeet Kumar Mishra: conceptualisation, data curation, methodology, investigation, visualisation, editing original draft, and supervision.

Conflicts of interest

The author declares that they have no known competing financial interests or personal relationships that could have appeared to influence the study reported in the present study.

Data availability

The datasets generated and/or analysed during the current study are not publicly available but are available from the corresponding author on reasonable request.

Acknowledgements

The author would like to thank the Biomass, Bioenergy and Bioproducts Lab, Department of Chemical Engineering, Manipal Institute of Technology, Manipal, Karnataka, India, for providing the necessary facilities.

References

1 R. Jadhav, *Reuters*, 2025, **https://www.reuters.com/sustainability/climate-energy/indias-ethanol-drive-imperils-its-push-edible-oil-self-sufficiency-2025-08-12/**.
2 N. Kathait, 2025, **https://www.spglobal.com/commodity-insights/en/news-research/latest-news/agriculture/061125-india-likely-to-emerge-as-key-ddgs-supplier-amid-ethanol-industry-expansion**.
3 A. Iram, D. Cekmecelioglu and A. Demirci, *Appl. Microbiol. Biotechnol.*, 2020, **104**, 6115–6128.
4 A. P. B. Fruet, J. L. Nörnberg, C. R. Calkins and A. De Mello, *Meat Sci.*, 2019, **154**, 119–125.
5 J. Lv, X. Ao, Q. Li, Y. Cao, Q. Chen and Y. Xie, *Bioresour. Technol.*, 2019, **283**, 59–66.
6 Q. Zheng, B. Lin, Q. Zhang, S. Wu, S. Wang, X. He, Y. Wang, X. Guan and X. Huang, *Energy Fuels*, 2015, **29**, 4305–4310.
7 Y. X. Pang, D. C. Foo, Y. Yan, N. Sharmin, E. Lester, T. Wu and C. H. Pang, *J. Anal. Appl. Pyrolysis*, 2021, **154**, 104995.
8 A. Kumar, Monika, R. K. Mishra and S. Jaglan, *Process Saf. Environ. Prot.*, 2022, **163**, 68–81.
9 B. Zhang, Z. Zhong, T. Li, Z. Xue, X. Wang and R. Ruan, *J. Anal. Appl. Pyrolysis*, 2018, **130**, 1–7.
10 R. K. Mishra and K. Mohanty, *Bioresour. Technol.*, 2020, **311**, 123480.
11 M. Heydari, M. Rahman and R. Gupta, *Int. J. Chem. Eng.*, 2015, **2015**, 481739.
12 M. V. Navarro, J. M. López, A. Veses, M. Callén and T. García, *Energy*, 2018, **165**, 731–742.
13 A. A. Jain, A. Mehra and V. V. Ranade, *Fuel*, 2016, **165**, 490–498.
14 P. De Filippis, B. De Caprariis, M. Scarsella and N. Verdone, *Energies*, 2015, **8**, 1730–1744.
15 R. Xiao, W. Yang, X. Cong, K. Dong, J. Xu, D. Wang and X. Yang, *Energy*, 2020, **201**, 117537.
16 H. Stančin, H. Mikulčić, N. Manić, D. Stojiljiković, M. Vujanović, X. Wang and N. Duić, *Energy*, 2021, **237**, 121592.
17 D. B. Pal, N. Srivastava, S. L. Pal, M. Kumar, A. Syed, A. M. Elgorban, R. Singh and V. K. Gupta, *Bioresour. Technol.*, 2021, **341**, 125891.
18 M. Kumar, D. Rai, G. Bhardwaj, S. N. Upadhyay and P. K. Mishra, *Ind. Crops Prod.*, 2021, **174**, 114128.
19 R. K. Mishra and K. Mohanty, *Biomass Convers. Biorefin.*, 2018, **8**, 799–812.
20 T. Bridgeman, L. Darvell, J. Jones, P. Williams, R. Fahmi, A. Bridgwater, T. Barraclough, I. Shield, N. Yates and S. Thain, *Fuel*, 2007, **86**, 60–72.
21 P. u. Van Soest, *J. - Assoc. Off. Anal. Chem.*, 1967, **50**, 50–55.
22 S. A. El-Sayed and M. E. Mostafa, *Energy Convers. Manage.*, 2014, **85**, 165–172.
23 S. Ceylan and D. Kazan, *Bioresour. Technol.*, 2015, **187**, 1–5.
24 V. Anand, R. Gautam and R. Vinu, *Fuel*, 2017, **205**, 1–10.
25 S. Vyazovkin, A. K. Burnham, J. M. Criado, L. A. Pérez-Maqueda, C. Popescu and N. Sbirrazzuoli, *Thermochim. Acta*, 2011, **520**, 1–19.
26 C. Gai, Y. Dong and T. Zhang, *Bioresour. Technol.*, 2013, **127**, 298–305.
27 M. Starink, *Thermochim. Acta*, 1996, **288**, 97–104.
28 T. Damartzis, D. Vamvuka, S. Sfakiotakis and A. Zabaniotou, *Bioresour. Technol.*, 2011, **102**, 6230–6238.
29 T. Raj, M. Kapoor, R. Gaur, J. Christopher, B. Lamba, D. K. Tuli and R. Kumar, *Energy Fuels*, 2015, **29**, 3111–3118.
30 F. G. Fonseca, A. Funke, A. Niebel, A. P. S. Dias and N. Dahmen, *J. Anal. Appl. Pyrolysis*, 2019, **139**, 73–86.
31 L. Basile, A. Tugnoli, C. Stramigioli and V. Cozzani, *Thermochim. Acta*, 2016, **636**, 63–70.
32 L. Puri, Y. Hu and G. Naterer, *Front. Fuels*, 2024, **2**, 1378361.
33 X. Hu, H. Guo, M. Gholizadeh, B. Sattari and Q. Liu, *Biomass Bioenergy*, 2019, **120**, 28–39.
34 Z. Zha, K. Wu, Z. Ge, Y. Ma, M. Zeng, Y. Wu, Y. Tao and H. Zhang, *Combust. Flame*, 2023, **247**, 112481.
35 S. Xu, J. Chen, H. Peng, S. Leng, H. Li, W. Qu, Y. Hu, H. Li, S. Jiang and W. Zhou, *Fuel*, 2021, **291**, 120128.
36 J. Sun, J. Luo, R. Ma, J. Lin and L. Fang, *Chemosphere*, 2023, **314**, 137680.
37 M. Wang, S.-L. Zhang and P.-G. Duan, *Energy Sources, Part A*, 2023, **45**, 2637–2650.
38 A. El Hanandeh, A. Albalasmeh and M. Gharaibeh, *Biomass Bioenergy*, 2021, **151**, 106163.
39 L. Zhu and Z. Zhong, *Korean J. Chem. Eng.*, 2020, **37**, 1660–1668.
40 A. Korus, J.-P. Gutierrez, A. Szlęk, J. Jagiello and A. Hornung, *Chem. Eng. J.*, 2022, **446**, 137298.
41 H. W. Ryu, H. W. Lee, J. Jae and Y.-K. Park, *Energy*, 2019, **179**, 669–675.
42 B. Gudka, L. Darvell, J. Jones, A. Williams, P. Kilgallon, N. Simms and R. Laryea-Goldsmith, *Fuel Process. Technol.*, 2012, **94**, 123–130.

43 T. Bunma and P. Kuchonthara, *Process Saf. Environ. Prot.*, 2018, **118**, 188–194.
44 S. Deng, X. Wang, J. Zhang, Z. Liu, H. Mikulčić, M. Vujanović, H. Tan and N. Duić, *J. Environ. Manage.*, 2018, **218**, 50–58.
45 H. Ghazidin, M. Z. E. Prayoga, H. P. Putra, U. Priyanto, A. Prismantoko and A. Darmawan, *Therm. Sci. Eng. Prog.*, 2023, **40**, 101769.
46 G. Bhardwaj, M. Kumar, P. K. Mishra and S. N. Upadhyay, *Biomass Convers. Biorefin.*, 2023, **13**, 3087–3100.
47 M. Kumar, S. K. Shukla, S. Upadhyay and P. Mishra, *Bioresour. Technol.*, 2020, **310**, 123393.
48 E. Apaydın Varol and Ü. Mutlu, *Energies*, 2023, **16**, 3674.
49 O. Senneca, F. Cerciello, C. Russo, A. Wütscher, M. Muhler and B. Apicella, *Fuel*, 2020, **271**, 117656.
50 G. Martínez-Narro, N. J. Royston, K. L. Billsborough and A. N. Phan, *Chem. Thermodyn. Therm. Anal.*, 2023, **9**, 100105.
51 P. Giudicianni, V. Gargiulo, C. M. Grottola, M. Alfè, A. I. Ferreiro, M. A. A. Mendes, M. Fagnano and R. Ragucci, *Energy Fuels*, 2021, **35**, 5407–5478.
52 S. He, W. Fu, Y. Wu, B. Sun, Q. Ling, Z. Cheng, B. Yan, G. Chen and S. Wang, *J. Anal. Appl. Pyrolysis*, 2025, **186**, 106926.
53 S. Wang, Y. Wu, B. Sun, S. He, Q. Ling, Z. Cheng, B. Yan and G. Chen, *J. Anal. Appl. Pyrolysis*, 2024, **177**, 106372.
54 R. Liu, G. Liu, B. Yousaf, Z. Niu and Q. Abbas, *Renewable Sustainable Energy Rev.*, 2022, **153**, 111761.
55 H. Chen, Y. Xie, W. Chen, M. Xia, K. Li, Z. Chen, Y. Chen and H. Yang, *Energy Convers. Manage.*, 2019, **196**, 320–329.
56 E. Müsellim, M. H. Tahir, M. S. Ahmad and S. Ceylan, *Appl. Therm. Eng.*, 2018, **137**, 54–61.
57 D. Cui, X. Zheng, J. Zou, S. Yu, X. Kong, J. Cai and X. Zhang, *Combust. Sci. Technol.*, 2024, **196**, 4181–4203.
58 M. Kumar, S. Sabbarwal, P. K. Mishra and S. N. Upadhyay, *Bioresour. Technol.*, 2019, **279**, 262–270.
59 G. Bianco and C. Leal Marchena, *Biofuels*, 2025, 1–8.
60 R. K. Mishra, S. Chinnam and A. Sharma, *Bioresour. Technol. Rep.*, 2024, **27**, 101899.
61 M. Kumar, D. Rai, G. Bhardwaj, S. Upadhyay and P. Mishra, *Ind. Crops Prod.*, 2021, **174**, 114128.
62 W.-H. Chen, C. F. Eng, Y.-Y. Lin and Q.-V. Bach, *Energy Convers. Manage.*, 2020, **221**, 113165.
63 L. Luo, X. Guo, Z. Zhang, M. Chai, M. M. Rahman, X. Zhang and J. Cai, *Energy Fuels*, 2020, **34**, 4874–4881.
64 J. E. White, W. J. Catallo and B. L. Legendre, *J. Anal. Appl. Pyrolysis*, 2011, **91**, 1–33.
65 R. K. Mishra and K. Mohanty, *Bioresour. Technol.*, 2018, **251**, 63–74.
66 D. Chen, K. Cen, X. Zhuang, Z. Gan, J. Zhou, Y. Zhang and H. Zhang, *Combust. Flame*, 2022, **242**, 112142.
67 Z. Zhang, H. Duan, Y. Zhang, X. Guo, X. Yu, X. Zhang, M. M. Rahman and J. Cai, *Energy*, 2020, **207**, 118290.
68 R. K. Mishra, Q. Lu and K. Mohanty, *J. Anal. Appl. Pyrolysis*, 2020, **150**, 104887.
69 A. Nawaz, R. K. Mishra, S. Sabbarwal and P. Kumar, *Bioresour. Technol. Rep.*, 2021, 100858.
70 A. Nawaz and P. Kumar, *Bioresour. Technol.*, 2021, **340**, 125722.
71 M. Kumar, S. Sabbarwal, P. Mishra and S. Upadhyay, *Bioresour. Technol.*, 2019, **279**, 262–270.
72 O. Y. Fetisova, N. M. Mikova and O. P. Taran, *Kinet. Catal.*, 2020, **61**, 846–853.
73 A. Nawaz and P. Kumar, *Bioresour. Technol.*, 2023, **376**, 128846.
74 X. Yuan, T. He, H. Cao and Q. Yuan, *Renewable Energy*, 2017, **107**, 489–496.
75 A. S. Khan, Z. Man, M. A. Bustam, C. F. Kait, Z. Ullah, A. Nasrullah, M. I. Khan, G. Gonfa, P. Ahmad and N. Muhammad, *J. Mol. Liq.*, 2016, **223**, 754–762.
76 M. Ivanovski, A. Petrovic, I. Ban, D. Goricanec and D. Urbancl, *Materials*, 2021, **14**, 7877.